ANZIAM J. **63** (2021), 420–433
doi:10.1017/S1446181121000353

NUMERICAL SOLUTIONS TO A FRACTIONAL DIFFUSION EQUATION USED IN MODELLING DYE-SENSITIZED SOLAR CELLS

BENJAMIN MALDON[1], BISHNU PRASAD LAMICHHANE[1] and NGAMTA THAMWATTANA[1]

(Received 21 October, 2020; accepted 16 July, 2021; first published online 16 November, 2021)

Abstract

Dye-sensitized solar cells consistently provide a cost-effective avenue for sources of renewable energy, primarily due to their unique utilization of nanoporous semiconductors. Through mathematical modelling, we are able to uncover insights into electron transport to optimize the operating efficiency of the dye-sensitized solar cells. In particular, fractional diffusion equations create a link between electron density and porosity of the nanoporous semiconductors. We numerically solve a fractional diffusion model using a finite-difference method and a finite-element method to discretize space and an implicit finite-difference method to discretize time. Finally, we calculate the accuracy of each method by evaluating the numerical errors under grid refinement.

2020 *Mathematics subject classification*: 35R11.

Keywords and phrases: dye-sensitized solar cells, electron density, efficiency, fractional diffusion, finite-difference methods, finite-element methods.

1. Introduction

Photoelectrochemical studies in dye-sensitized solar cells (DSSCs) have remained vibrant since their officially recognized introduction in O'Regan and Grätzel's seminal paper [34]. DSSCs relieve traditional solar cell designs of their dependence on high-purity semiconductors such as silicon, opting instead for the significantly cheaper titanium dioxide (TiO_2). Typically, DSSCs utilize four primary components to generate sunlight: a photosensitive dye, a nanoporous semiconductor, a counter electrode and an electrolyte couple [34].

[1]School of Mathematical and Physical Sciences, University of Newcastle, Callaghan, NSW 2308, Australia; e-mail: benjamin.maldon@uon.edu.au, bishnu.lamichhane@newcastle.edu.au and natalie.thamwattana@newcastle.edu.au.

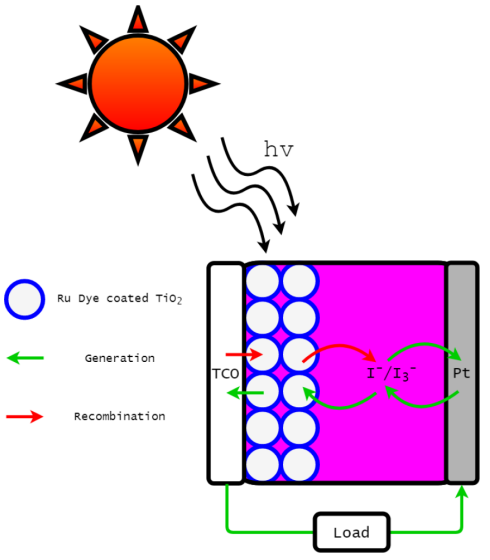

FIGURE 1. Diagram of an operating dye-sensitized solar cell [28] (colour available online).

Sunlight excites the dye molecules, which inject electrons to the nanoporous semiconductor. Injected electrons are sent to power a load and are reintroduced into the DSSC via the counter electrode. Finally, the electrolyte couple transfers electrons from the counter electrode back to the photosensitive dye by a pair of redox reactions.

DSSCs are liable to suffer recombination effects. Injected electrons may be absorbed by the dye or regenerate the electrolyte couple instead of powering the load, which reduces the overall effectiveness of the device. Figure 1 shows a DSSC in operation, denoting the processes encouraging electricity generation by green arrows and recombination by red arrows [28].

Södergren et al. [36] pioneered diffusion-based mathematical modelling for DSSCs, using the electron density to calculate the current–voltage relationship and the efficiency of a given DSSC. Cao et al. [7] augmented the diffusion model with time dependence and introduced nonlinear diffusivity to capture the role of trap states in the TiO_2 network, which was studied further by Anta et al. [2] and Maldon et al. [25].

Nigmatullin [33] proposed one of the first fractional diffusion models to study the influence of the fractal geometry of a material on its diffusion processes (particularly, the transfer equation for particles in a porous medium). Nelson [31] and Benkstein et al. [5] explored the electron diffusion process on TiO_2, with the latter motivated by its effect on DSSCs. Benkstein et al. [5] established a critical link between the porosity of the TiO_2, its resultant fractal geometry and the electron transport in TiO_2 with continuous-time random walk (CTRW) simulations. Henry and Wearne [18] developed a sub-diffusion equation based on CTRW simulations to create a novel fractional partial differential equation (FPDE), from which Maldon and Thamwattana

https://doi.org/10.1017/S1446181121000353 Published online by Cambridge University Press

[27] derived a new fractional diffusion equation for DSSCs that accounted for the fractal geometry of the TiO_2 semiconductor.

Fractional diffusion equations are well posed and special cases of pure diffusion also possess analytical solutions [23]. Chen et al. [9] used separation of variables to analytically solve the time-fractional heat equation on a bounded spatial domain. Tomovski and Sandev [38] analytically solved the generalized time-fractional diffusion equation under a variety of boundary conditions.

Laplace transform methods remain a popular method for numerically solving FPDEs, as fractional derivatives are well suited for Laplace transformation [6]. Duan et al. [11] also used Laplace transform methods to numerically solve fractional diffusion-wave equations.

Spline collocation methods are also commonly employed to numerically solve fractional diffusion problems. Maldon et al. [26] provided numerical solutions with a cubic B-spline method to discretize space and an implicit finite-difference method to discretize time. El Danaf [12] used spline functions to numerically solve the time-fractional and space-fractional diffusion equation on a bounded interval under Dirichlet boundary conditions. Zahra and Elkholy [41] applied cubic B-splines to numerically solve a fractional ordinary differential equation which was used to model fluid flow.

In this paper, we numerically solve a fractional diffusion model. We discretize space with a finite-difference method and a finite-element method and discretize time using an implicit finite-difference method. To elucidate the effectiveness of each scheme, we estimate the numerical errors by comparison to a fine grid solution to serve as a pseudo-analytical solution.

2. Mathematical model

Given a DSSC of thickness d, the electron density $n(x,t)$ at position $x \in [0,d]$ and time $t \geq 0$ satisfies the FPDE [27]

$$\frac{\partial n}{\partial t} = D_0 \frac{\partial^{1-\gamma}}{\partial t^{1-\gamma}} \frac{\partial^2 n}{\partial x^2} + \varphi \alpha e^{-\alpha x} - k_R(n(x,t) - n_{\text{eq}}), \tag{2.1}$$

where D_0 is the diffusion coefficient, γ is the exponent in the mean-square displacement of the CTRW simulation of the semiconductor, φ is the incident photon flux, α is the dye absorption coefficient, k_R is the recombination constant and n_{eq} is the dark equilibrium electron density. Equation (2.1) is subject to the boundary conditions

$$n(0,t) = n_0 = n_{\text{eq}} e^{qV_B/m_I k_B T}, \tag{2.2}$$

$$\left.\frac{\partial n}{\partial x}\right|_{x=d} = 0, \tag{2.3}$$

$$n(x,0) = n_0, \tag{2.4}$$

where q is the electron charge, V_B is the bias voltage, m_I is the diode ideality factor, k_B is Boltzmann's constant [3] and T is the temperature of the DSSC.

https://doi.org/10.1017/S1446181121000353 Published online by Cambridge University Press

We note that under the special case $\gamma = 1$, we recover the standard linear diffusion model studied by Maldon et al. [25], as the mean-square displacement in CTRW simulations is usually proportional to time [18]. Given that the exponents β in the mean-square displacement (studied by Benkstein et al. [5]) lie in the range $0 < \beta \leq 0.5$, this model only considers sub-diffusion ($0 < \gamma \leq 1$). Lower values of γ result in fewer electron jumps, which consequently slows the diffusion process [5].

In this paper, we employ the Caputo fractional derivative [8] for its easy adoption of traditional boundary conditions [15, 27]. Langlands et al. [20] noted that the use of the Riemann–Liouville fractional derivative leads to an FPDE that is not positivity preserving (see also the article by Baeumer et al. [4]). Without a spatially dependent source term, Langlands et al. [20] suggested the alternative FPDE

$$\frac{\partial n}{\partial t} = D_0 e^{-kt} \frac{\partial^{1-\gamma}}{\partial t^{1-\gamma}} \left(e^{kt} \frac{\partial^2 n}{\partial x^2} \right) - kn,$$

where k is the reaction coefficient. For other fractional reaction–diffusion equations featuring the Riemann–Liouville derivative and the influence of chemical reactions, we refer the reader to the work of Méndez et al. [30, Section 3.4]. We also refer the reader to the paper by Meerschaert and Sikorskii [29, Ch. 7] for the Langlands model, which is another model to study CTRW motion.

The diode equation is commonly used to compute the current–density relationship for solar cells, in which the current J as a function of bias voltage V_B is given by [36]

$$J(V_B) = J_{\text{sc}} - J_0(e^{qV_B/m_I k_B T - 1}),$$

where J_0 is the dark saturation current density, given by

$$J_0 = q n_{\text{eq}} \sqrt{D_0 k_R} \tanh\left(\sqrt{\frac{k_R}{D_0}} d \right).$$

To compute the short-circuit current density J_{sc}, we use

$$J_{\text{sc}} = q D_0 \left[\frac{\partial^{1-\gamma}}{\partial t^{1-\gamma}} \left(\frac{\partial n}{\partial x} \right) \right] \Bigg|_{x=0},$$

noting that the usual electron flux is recovered in the linear diffusion special case $\gamma = 1$.

Given that the open-circuit voltage V_{oc} satisfies $J(V_{\text{oc}}) = 0$, we may compute the open-circuit voltage with

$$V_{\text{oc}} = \frac{m_I k_B T}{q} \ln\left(\frac{J_{\text{sc}}}{J_0} + 1 \right).$$

Maximizing the power output $P(V_B) = V_B J(V_B)$ over V_B, we obtain the maximum power point V_{max} by

$$V_{\text{max}} = \frac{m_I k_B T}{q} \left(W\left(e \frac{J_{\text{sc}} + J_0}{J_0} \right) - 1 \right),$$

https://doi.org/10.1017/S1446181121000353 Published online by Cambridge University Press

TABLE 1. Parameter values for the numerical simulation.

Parameter	Value	Unit	Reference
γ	0.612	–	[5]
D_0	10^{-11}	$m^2\,s^{-1}$	[2]
α	10^5	m^{-1}	[14]
d	5×10^{-5}	m	[2]
k_R	4×10^{-8}	s^{-1}	[2]
n_{eq}	10^{22}	m^{-3}	[32]
φ	10^{21}	$m^{-2}\,s^{-1}$	[16]
V_B	0	V	–
P_i	1000	$W\,m^{-2}$	[14]

where W is the Lambert W-function [27] and $J_{\max} = J(V_{\max})$. With $P_{\max} = V_{\max}J_{\max}$, we compute the efficiency η of the DSSC by

$$\eta = \frac{P_{\max}}{P_i}, \tag{2.5}$$

where P_i is the power of incident light.

In this paper, we use parameter values presented in Table 1 to numerically solve equation (2.1) unless otherwise stated.

3. Numerical methods

Let $t_f > 0$ be the final simulation time. Discretizing $[0, t_f]$ into N_t temporal nodes and $[0, d]$ into N_x spatial nodes, we let

$$\Delta x = \frac{d}{N_x - 1}, \quad \Delta t = \frac{t_f}{N_t - 1}, \quad x_k = (k-1)\Delta x, \quad t_m = (m-1)\Delta t$$

for each $k = 1, \ldots, N_x + 1$ and $m = 1, \ldots, N_t$. To numerically estimate the fractional derivative of a function f of order $1-\gamma$, we use [35]

$$\left.\frac{\partial^{1-\gamma} f}{\partial t^{1-\gamma}}\right|_{t=t_m} = \frac{(\Delta t)^{\gamma-1}}{\Gamma(\gamma+1)} \sum_{p=0}^{m-2} [(p+1)^{\gamma} - p^{\gamma}][f(t_{m-p}) - f(t_{m-p-1})] + \mathbf{O}\Delta t, \tag{3.1}$$

where Γ denotes the usual Gamma function

$$\Gamma(z) = \int_0^{\infty} x^{z-1} e^{-x} dx.$$

The finite-difference approximation given in equation (3.1) provides a first-order estimate for the fractional time derivative [13]. By using an implicit finite-difference method to discretize time, we obtain an unconditionally stable numerical solution [19]. For a second-order approximation, we refer the reader to the paper by Dimitrov [10].

https://doi.org/10.1017/S1446181121000353 Published online by Cambridge University Press

3.1. Finite-difference method To solve equation (2.1) under the boundary conditions (2.2)–(2.4), we use a finite-difference method (FDM) to discretize space and equation (3.1) to discretize time. In the literature, Esen et al. [13] numerically solved the space–time fractional heat equation. Yuste and Acedo [40] proposed an explicit and conditionally stable FDM scheme using Grünwald–Letnikov discretization for the fractional derivative. Lynch et al. [24] employed a semi-implicit finite-difference method for solving FPDEs, which outperforms standard explicit methods on stability and accuracy. For further details on the consistency, stability and convergence properties of FDM schemes for numerically solving FPDEs, we refer the reader to Li and Zeng's review paper [22]. To account for the Neumann boundary condition at $x = d$, we also employ a 'ghost node' at $x = d + \Delta x$. Let $y_{m,k}$ denote the numerical solution at (x_k, t_m). That is,

$$n(x_k, t_m) \approx y_{m,k}$$

for each $k = 1, \ldots, N_x + 1$ and $m = 1, \ldots, N_t$.

3.1.1. Nodes determined by boundary conditions. To satisfy the initial condition (2.4), we set

$$y_{1,k} = n_0$$

for all $k = 1, \ldots, N_x$. For the Dirichlet boundary condition (2.2) at $x = 0$, we set

$$y_{m,1} = n_0$$

for all $m = 1, \ldots, N_t$. Finally, for the Neumann boundary condition (2.3) at $x = d$, we use a central difference approximation for the first derivative at $x = d$ to set

$$y_{m,Nx+1} = y_{m,Nx-1}$$

for all $m = 1, \ldots, N_t$. Here $N_x + 1$ corresponds to the ghost node at $x = d + \Delta x$.

3.1.2. Algorithm. For each $m = 2, \ldots, N_t$, we set

$$\left[\frac{\partial n}{\partial t}\right]\Bigg|_{t=t_m, x=x_k} = D_0\left[\frac{\partial^{1-\gamma}}{\partial t^{1-\gamma}}\frac{\partial^2 n}{\partial x^2}\right]\Bigg|_{t=t_m, x=x_k} + \varphi\alpha e^{-\alpha x_k} - k_R(n(x_k, t_m) - n_{eq}).$$

Using the backward Euler method [17], a central difference approximation and equation (3.1) to estimate $\partial n/\partial t$, $\partial^2 n/\partial x^2$ and the fractional derivative, respectively,

$$\begin{aligned}\frac{y_{m,k} - y_{m-1,k}}{\Delta t} = {} & \frac{D_0(\Delta t)^{\gamma-1}}{\Gamma(\gamma+1)}\sum_{p=0}^{m-2}[(p+1)^\gamma - p^\gamma] \\ & \times\left[\frac{y_{m-p,k-1} - 2y_{m-p,k} + y_{m-p,k+1}}{(\Delta x)^2} - \frac{y_{m-p-1,k-1} - 2y_{m-p-1,k} + y_{m-p-1,k+1}}{(\Delta x)^2}\right] \\ & + \varphi\alpha e^{-\alpha x_k} - k_R(n(x_k, t_m) - n_{eq}).\end{aligned}$$

https://doi.org/10.1017/S1446181121000353 Published online by Cambridge University Press

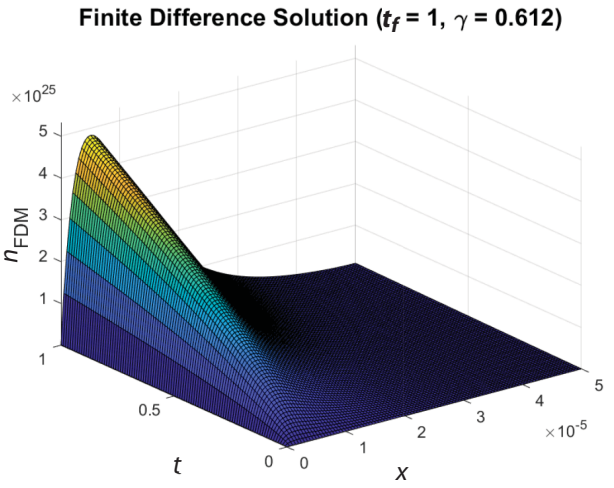

FIGURE 2. Plot of the numerical solution to equation (2.1) under (2.2)–(2.4) using the FDM scheme.

Upon simplification,

$$
\begin{aligned}
&-\frac{D_0(\Delta t)^\gamma}{\Gamma(\gamma+1)(\Delta x)^2}y_{m,k-1}+\left[1+k_R\Delta t+\frac{2D_0(\Delta t)^\gamma}{\Gamma(\gamma+1)(\Delta x)^2}\right]y_{m,k}-\frac{D_0(\Delta t)^\gamma}{\Gamma(\gamma+1)(\Delta x)^2}y_{m,k+1}\\
&\quad=-\frac{D_0(\Delta t)^\gamma}{\Gamma(\gamma+1)(\Delta x)^2}[y_{m-1,k-1}-2y_{m-1,k}+y_{m-1,k+1}]+\frac{D_0(\Delta t)^{\gamma-1}}{\Gamma(\gamma+1)}\sum_{p=1}^{m-2}[(p+1)^\gamma-p^\gamma]\\
&\qquad\times\left[\frac{y_{m-p,k-1}-2y_{m-p,k}+y_{m-p,k+1}}{(\Delta x)^2}-\frac{y_{m-p-1,k-1}-2y_{m-p-1,k}+y_{m-p-1,k+1}}{(\Delta x)^2}\right]\\
&\qquad+\varphi\alpha e^{-\alpha x_k}-k_R(n(x_k,t_m)-n_{eq}),
\end{aligned}
$$

which results in N_x+1 equations in N_x+1 unknowns, when combined with the boundary conditions (2.2) and (2.3).

Figure 2 shows the numerical solution to (2.1) under boundary conditions (2.2)–(2.4) using the data from Table 1, $N_x=100$, $N_t=100$ and $t_f=1$. From Figure 2, we see that the electron density assumes its shape from the interaction of the Dirichlet boundary condition, the exponential source term and diffusion. Note that Figure 2 shows good agreement with the explicit finite-difference method used by Maldon and Thamwattana [27] while significantly improving stability with the use of an implicit finite-difference method.

3.2. Finite-element method We also solve equation (2.1) under (2.2)–(2.4) using a finite-element method (FEM) adapted from Alberty et al. [1]. Esen et al. [13] provided a finite-element basis for the time-fractional diffusion equation under Dirichlet boundary conditions. Yuan and Chen [39] solved a mixed diffusion problem featuring the two-sided Riemann–Liouville fractional derivatives by an FEM scheme. Li and

https://doi.org/10.1017/S1446181121000353 Published online by Cambridge University Press

Wang [21] solved time-fractional reaction–diffusion and diffusion-wave equations, using Galerkin FEM schemes [37] which enjoy unconditional stability.

3.2.1. Weak formulation. Letting $\rho = n - n_0$, we solve the equivalent problem

$$\frac{\partial \rho}{\partial t} = D_0 \frac{\partial^{1-\gamma}}{\partial t^{1-\gamma}} \frac{\partial^2 \rho}{\partial x^2} + \varphi \alpha e^{-\alpha x} - k_R(\rho + n_0 - n_{eq}), \tag{3.2}$$

subject to

$$\begin{aligned} \rho(x, 0) &= 0, \\ \rho(0, t) &= 0, \\ \left.\frac{\partial \rho}{\partial x}\right|_{x=d} &= 0. \end{aligned}$$

Upon multiplying by a test function w and integrating over $[0, d]$,

$$\begin{aligned} \int_0^d \frac{\partial \rho}{\partial t} w \, dx = D_0 \int_0^d \frac{\partial^{1-\gamma}}{\partial t^{1-\gamma}} \frac{\partial^2 \rho}{\partial x^2} w \, dx \\ + \int_0^d (\varphi \alpha e^{-\alpha x} - k_R(n_0 - n_{eq})) w \, dx - k_R \int_0^d \rho \, w \, dx. \end{aligned}$$

Integrating by parts and using the commutativity of the Caputo derivative,

$$\int_0^d \frac{\partial^{1-\gamma}}{\partial t^{1-\gamma}} \frac{\partial^2 \rho}{\partial x^2} w \, dx = \left[\frac{\partial^{1-\gamma}}{\partial t^{1-\gamma}} \left(\frac{\partial \rho}{\partial x} \right) w \right]_0^d - \int_0^d \frac{\partial^{1-\gamma}}{\partial t^{1-\gamma}} \frac{\partial \rho}{\partial x} \frac{dw}{dx} dx.$$

Given that $w(0) = 0$ and $(\partial \rho / \partial x)|_{x=d} = 0$, the weak formulation for equation (3.2) is given by

$$\begin{aligned} \int_0^d \frac{\partial \rho}{\partial t} w \, dx = -D_0 \int_0^d \frac{\partial^{1-\gamma}}{\partial t^{1-\gamma}} \frac{\partial \rho}{\partial x} \frac{\partial w}{\partial x} \, dx \\ + \int_0^d (\varphi \alpha e^{-\alpha x} - k_R(n_0 - n_{eq})) w \, dx - k_R \int_0^d \rho \, w \, dx. \end{aligned}$$

To solve equation (3.2) using this weak formulation, we employ the basis $\{\phi_1, \phi_2, \ldots, \phi_{N_x - 1}\}$, where ϕ_j is given by

$$\phi_j(x) = \begin{cases} \dfrac{x - x_j}{\Delta x} & x_j < x \le x_{j+1}, \\ \dfrac{x_{j+2} - x}{\Delta x} & x_{j+1} < x \le x_{j+2}, \\ 0 & \text{otherwise}, \end{cases}$$

for $j = 1, \ldots, N_x - 2$ and $\phi_{N_x - 1}$ is given by

$$\phi_{N_x - 1}(x) = \begin{cases} \dfrac{x - x_{N_x - 1}}{\Delta x} & x_{N_x - 1} < x \le d, \\ 0 & \text{otherwise}. \end{cases}$$

https://doi.org/10.1017/S1446181121000353 Published online by Cambridge University Press

3.3. Algorithm At each time step t_m, we set

$$\rho(x, t_m) \approx P(x, t_m) \sum_{j=1}^{N_x-1} g_j(t_m)\phi_j(x),$$

where g_j are the coefficients of the basis functions. In matrix form, the weak formulation of equation (3.2) under the basis $\{\phi_1, \phi_2, \ldots, \phi_{N_x-1}\}$ is given by

$$M\frac{\partial \vec{g}}{\partial t} = -D_0 A \frac{d^{1-\gamma}\vec{g}}{dt^{1-\gamma}} - k_R M\vec{g} + \vec{C},$$

where the coefficient vector $\vec{g}$, the mass matrix M, the stiffness matrix A and the load vector $\vec{C}$ components are given by

$$\begin{aligned}
\vec{g}_m &= [g_1(t_m), g_2(t_m), \ldots, g_{N_x-1}(t_m)],\\
M_{i,j} &= \int_0^d \phi_i(x)\phi_j(x)\,dx,\\
A_{i,j} &= \int_0^d \frac{d\phi_i}{dx}\frac{d\phi_j}{dx}\,dx,\\
\vec{C}_j &= \int_0^d [\varphi\alpha e^{-\alpha x} - k_R(n_0 - n_{eq})]\phi_j(x)\,dx
\end{aligned}$$

for each $m = 1, \ldots, N_t$, $i = 1, \ldots, N_x - 1$ and $j = 1, \ldots, N_x - 1$. Applying the implicit finite-difference method to discretize time, we obtain the system

$$A_L\vec{g}_m = A_c\vec{g}_{m-1} + A_R\sum_{p=1}^{m-2}[(p+1)^\gamma - p^\gamma][\vec{g}_{m-p} - \vec{g}_{m-p-1}] + \Delta t\vec{C},$$

where

$$\begin{aligned}
A_L &= (1 + k_R\Delta t)M + \frac{D_0(\Delta t)^\gamma}{\Gamma(\gamma+1)}A,\\
A_C &= k_R(\Delta t)M + \frac{D_0(\Delta t)^\gamma}{\Gamma(\gamma+1)}A,\\
A_R &= -\frac{D_0(\Delta t)^\gamma}{\Gamma(\gamma+1)}A.
\end{aligned}$$

Figure 3 shows the numerical solution to equation (2.1) under the conditions (2.2)–(2.4) using the data from Table 1, $N_x = 100$, $N_t = 100$ and $t_f = 1$.

4. Efficiency calculations

To elucidate the effect of the TiO_2 nanoporous semiconductor on efficiency through the parameter γ, we calculate η using equation (2.5) and the numerical solution obtained by the finite-difference method.

https://doi.org/10.1017/S1446181121000353 Published online by Cambridge University Press

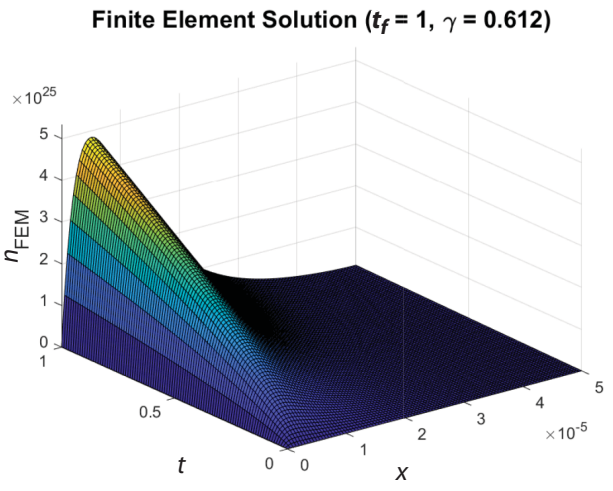

FIGURE 3. Plot of the numerical solution to equation (2.1) under (2.2)–(2.4) using the finite-element method.

4.1. Electron flux calculation To calculate the short-circuit current density, we estimate the time-fractional derivative with equation (3.1) and the electron flux at $x = 0$ with the 10-point estimate from Maldon and Thamwattana [27]. Therefore, under the finite-difference method the short-circuit current density is given by

$$J_{sc} = \frac{qD_0(\Delta t)^{\gamma-1}}{\Gamma(\gamma+1)} \sum_{p=0}^{N_t-2} [(p+1)^\gamma - p^\gamma] \Bigg[\sum_{j=1}^{10} a_j (y_{N_t-p,j} - y_{N_t-p-1,j}) \Bigg],$$

where each coefficient is given by

$$\begin{aligned} a_1 &= -\frac{7129}{2520\Delta x}, & a_2 &= \frac{9}{\Delta x}, & a_3 &= -\frac{18}{\Delta x}, \\ a_4 &= \frac{28}{\Delta x}, & a_5 &= -\frac{63}{2\Delta x}, & a_6 &= \frac{126}{5\Delta x}, \\ a_7 &= -\frac{14}{\Delta x}, & a_8 &= \frac{36}{7\Delta x}, & a_9 &= -\frac{9}{8\Delta x}, & a_{10} &= \frac{1}{9\Delta x}. \end{aligned}$$

4.1.1. Efficiency calculations. In Table 2, we calculate the efficiency η under several values for the parameter γ and the numerical data provided in Table 1. From the table, we see that efficiency decreases as γ increases, which is indicative of longer waiting times in the CTRW simulation [27].

5. Error calculation

In lieu of an analytical solution, we compute the accuracy of each method using a comparison to a fine grid solution from the same numerical method. We calculate the

https://doi.org/10.1017/S1446181121000353 Published online by Cambridge University Press

TABLE 2. Values for efficiency η (%) under several values of the parameter γ.

γ	$\eta(\%)$
0.25	3.6544
0.5	5.6951
0.612	6.6115
0.75	7.6690
1	8.4578

TABLE 3. Errors for the finite-difference method (FDM) and finite-element method (FEM) for solving equation (2.1) under temporal refinement given $N_x = 100$, using equation (5.1).

Scheme	$N_t = 8$	$N_t = 16$	$N_t = 32$	$N_t = 64$
FDM	0.2367	0.1177	0.0613	0.0335
FEM	0.2228	0.1039	0.0475	0.0197

TABLE 4. Errors for the finite-difference method (FDM) and finite-element method (FEM) for solving equation (2.1) under spatial refinement given $N_t = 1000$, using equation (5.1).

Scheme	$N_x = 16$	$N_x = 32$	$N_x = 64$	$N_x = 128$
FDM	0.2982	0.0786	0.0193	0.0046
FEM	0.3043	0.0675	0.0161	0.0040

errors for $t_f = 1$ under the parameter data in Table 1. For the reference solution, we use a finite-difference solution and finite element with 1000 spatial nodes and 1000 temporal nodes.

To calculate the error ϵ for both schemes under refinement, we use

$$\epsilon = \frac{\sqrt{\Delta x \Delta t}}{n_0} \|\vec{u}_C - \vec{u}_F\|, \tag{5.1}$$

where $\vec{u}_C$ is the coarse grid solution vector, $\vec{u}_F$ is the interpolated fine grid solution vector, Δx and Δt are calculated in the coarse grid and $\|\cdot\|$ denotes the usual root-mean-square error. We scale ϵ by n_0^{-1} to account for the high magnitude of the numerical solution.

From Table 3, we see that the error decreases by a factor of two when the number of temporal nodes doubles, which confirms that equation (3.1) provides a first-order approximation for the fractional time derivative in equation (2.1) for both numerical schemes. Table 4 shows that the error for both schemes decreases by a factor of four when the number of spatial nodes doubles, confirming that the finite-difference method and finite-element method provide second-order spatial discretizations. From

https://doi.org/10.1017/S1446181121000353 Published online by Cambridge University Press

Tables 3 and 4, we see that the finite-element scheme is consistently more accurate than the finite-difference scheme, since the weak formulation of the finite-element method naturally satisfies the Dirichlet and Neumann boundary conditions.

6. Summary

We solve the fractional partial differential equation (2.1) using a finite-difference method and a finite-element method to discretize space and an implicit finite-difference method to discretize time. Our numerical results are in good agreement with the literature. Error analysis indicates that the finite-difference method and finite-element method feature respectively first- and second-order spatial approximations while equation (3.1) provides an unconditionally stable finite- difference approximation for Caputo fractional derivatives of order $0 < \gamma \leq 1$.

Finally, we use the numerical schemes to compute the efficiency of a DSSC under several values of γ to elucidate the effect of electron diffusion in the nanoporous semiconductor. We find that lower values of γ lead to lower efficiencies due to the slower diffusion process associated with longer waiting times in the CTRW simulation.

Acknowledgements

This research has been conducted with the support of an Australian Government Research Training Program Scholarship. The authors are grateful to the Australian Research Council for the funding of Discovery Project DP170102705. The authors are also grateful for the suggestions made by the referees of this paper.

References

[1] J. Alberty, C. Carstensen and S. A. Funken, "Remarks around 50 lines of Matlab: short finite element implementation", *Numer. Algorithms* **20** (1999) 117–137; doi:10.1023/A:1019155918070.

[2] J. A. Anta, F. Casanueva and G. Oskam, "A numerical model for charge transport and recombination in dye-sensitized solar cells", *J. Phys. Chem. B* **110** (2006) 5372–5378; doi:10.1021/jp056493h.

[3] J. A. Anta, J. Idígoras, E. Guillén, J. Villanueva-Cab, H. J. Mandujano-Ramirez, G. Oskam, L. Pellejá and E. Palomares, "A continuity equation for the simulation of the current–voltage curve and the time-dependent properties of dye-sensitized solar cells", *Phys. Chem. Chem. Phys.* **14** (2012) 10285–10299; doi:10.1039/c2cp40719a.

[4] B. Baeumer, M. Kovács, M. Meerschaert and H. Sankaranarayanan, "Reprint of: Boundary conditions for fractional diffusion", *J. Comput. Appl. Math.* **339** (2018) 414–430; doi:10.1016/j.cam.2018.03.007.

[5] K. D. Benkstein, N. Kopidakis, J. van de Lagemaat and A. J. Frank, "Influence of the percolation network geometry on electron transport in dye-sensitized titanium dioxide solar cells", *J. Phys. Chem. B* **107** (2003) 7759–7767; doi:10.1021/jp0226811.

[6] R. G. Campos and A. Huet, "Numerical inversion of the Laplace transform and its application to fractional diffusion", *Appl. Math. Comput.* **327** (2018) 70–78; doi:10.1016/j.amc.2018.01.026.

[7] F. Cao, G. Oskam, G. J. Meyer and P. C. Searson, "Electron transport in porous nanocrystalline TiO_2 photoelectrochemical cells", *J. Phys. Chem.* **100** (1996) 17021–17027; doi:10.1021/jp9616573.

[8] M. Caputo, "Linear models of dissipation whose Q is almost frequency independent—II", *Geophys. J. Int.* **13** (1967) 529–539; doi:10.1111/j.1365-246X.1967.tb02303.x.

[9] Z. Q. Chen, M. M. Meerschaert and E. Nane, "Space–time fractional diffusion on bounded domains", *J. Math. Anal. Appl.* **393** (2012) 479–488; doi:10.1016/j.jmaa.2012.04.032.

[10] Y. Dimitrov, "A second order approximation for the Caputo fractional derivative", *J. Fract. Calc. Appl.* **7** (2016) 175–195; https://www.researchgate.net/publication/272022891_A_second_order_approximation_for_the_Caputo_fractional_derivative.

[11] J. S. Duan, S. Z. Fu and Z. Wang, "Fractional diffusion-wave equations on finite interval by Laplace transform", *Integral Transforms Spec. Funct.* **25** (2014) 220–229; doi:10.1080/10652469.2013.838759.

[12] T. S. El Danaf, "Numerical solution for the linear time and space fractional diffusion equation", *J. Vib. Control* **21** (2015) 1769–1777; doi:10.1177/1077546313500687.

[13] A. Esen, Y. Ucar, N. Yagmurlu and O. Tasbozan, "A Galerkin finite element method to solve fractional diffusion and fractional diffusion-wave equations", *Math. Model. Anal.* **18** (2013) 260–273; doi:10.3846/13926292.2013.783884.

[14] Y. Gacemi, A. Cheknane and H. S. Hilal, "Simulation and modelling of charge transport in dye-sensitized solar cells based on carbon nano-tube electrodes", *Phys. Scr.* **87** (2013) 035703–035714; doi:10.1088/0031-8949/87/03/035703.

[15] R. Garrappa, E. Kaslik and M. Popolizio, "Evaluation of fractional integrals and derivatives of elementary functions: overview and tutorial", *Mathematics* **7** (2019) 407–428; doi:10.3390/math7050407.

[16] R. Gómez and P. Salvador, "Photovoltage dependence on film thickness and type of illumination in nanoporous thin film electrodes according to a simple diffusion model", *Solar Energy Mater. Solar Cells* **88** (2005) 377–388; doi:10.1016/j.solmat.2004.11.008.

[17] G. W. Griffiths, *Numerical analysis using R: solutions to ODEs and PDEs* (Cambridge University Press, New York, 2016); doi:10.1017/CBO9781316336069.

[18] B. I. Henry and S. L. Wearne, "Fractional reaction–diffusion", *Physica A* **276** (2000) 448–455; doi:10.1016/S0378-4371(99)00469-0.

[19] T. A. M. Langlands and B. I. Henry, "The accuracy and stability of an implicit solution method for the fractional diffusion equation", *J. Comput. Phys.* **205** (2005) 719–736; doi:10.1016/j.jcp.2004.11.025.

[20] T. A. M. Langlands, B. I. Henry and S. L. Wearne, "Anomalous subdiffusion with multispecies linear reaction dynamics", *Phys. Rev. E* **77** (2008) 021111; doi:10.1103/PhysRevE.77.021111.

[21] C. Li and Z. Wang, "The local discontinuous Galerkin finite element methods for Caputo-type partial differential equations: numerical analysis", *Appl. Numer. Math.* **140** (2019) 1–22; doi:10.1016/j.apnum.2019.01.007.

[22] C. Li and F. Zeng, "Finite difference methods for fractional differential equations", *Internat. J. Bifur. Chaos Appl. Sci. Engrg.* **22** (2012) 1230014; doi:10.1142/S0218127412300145.

[23] Y. Luchko, "Initial value problems for the one-dimensional time-fractional diffusion equation", *Fract. Calc. Appl. Anal.* **15** (2012) 141–160; doi:10.2478/s13540-012-0010-7.

[24] V. E. Lynch, B. A. Carreras, D. del-Castillo-Negrete, K. M. Ferreira-Mejias and H. R. Hicks, "Numerical methods for the solution of partial differential equations of fractional order", *J. Comput. Phys.* **192** (2003) 406–421; doi:10.1016/j.jcp.2003.07.008.

[25] B. Maldon, B. P. Lamichhane and N. Thamwattana, "Numerical solutions for nonlinear partial differential equations arising from modelling dye-sensitized solar cells", *Proc. 18th Biennial Comput. Tech. Appl. Conf., CTAC-2018,* (eds B. Lamichhane, T. Tran and J. Bunder), (2019), C231–C246; doi:10.21914/anziamj.v60i0.14053.

[26] B. Maldon, B. P. Lamichhane and N. Thamwattana, "A cubic *B*-spline collocation method for numerically solving fractional diffusion equations used in modelling dye-sensitized solar cells", *Proc. 19th Biennial Comput. Tech. Appl. Conf., CTAC-2020* (eds W. McLean and S. MacNamara), (2020).

[27] B. Maldon and N. Thamwattana, "A fractional diffusion model for dye-sensitized solar cells", *Molecules* **25** (2020) 2966–2975; doi:10.3390/molecules25132966.

[28] B. Maldon, N. Thamwattana and M. Edwards, "Exploring nonlinear diffusion equations for modelling dye-sensitized solar cells", *Entropy* **22**(2) (2020) Article ID 248; doi:10.3390/e22020248.
[29] M. M. Meerschaert and A. Sikorskii, *Stochastic models for fractional calculus*, Volume 43 (De Gruyter, Berlin, 2012); doi:10.1515/9783110258165.
[30] V. Méndez, S. Fedotov and W. Horsthemke, *Reaction-transport systems* (Springer, Berlin, 2010); doi:10.1007/978-3-642-11443-4.
[31] J. Nelson, "Continuous-time random-walk model of electron transport in nanocrystalline TiO_2 electrodes", *Phys. Rev. B* **59** (1999) 15374–15380; doi:10.1103/PhysRevB.59.15374.
[32] M. Ni, M. K. H. Leung, D. Y. C. Leung and K. Sumathy, "An analytical study of the porosity effect on dye-sensitized solar cell performance", *Solar Energy Mater. Solar Cells* **90** (2006) 1331–1344; doi:10.1016/j.solmat.2005.08.006.
[33] R. Nigmatullin, "The realization of the generalized transfer equation in a medium with fractal geometry", *Phys. Stat. Sol. B* **133** (1986) 425–430; doi:10.1002/pssb.2221330150.
[34] B. O'Regan and M. Grätzel, "A low-cost, high-efficiency solar cell based on dye-sensitized colloidal TiO_2 films", *Nature* **353** (1991) 737–740; doi:10.1038/353737a0.
[35] K. Oldham and J. Spanier, *The fractional calculus: theory and applications of differentiation and integration to arbitrary order*, Volume 111 (Elsevier, New York, 1974); https://catalogue.nla.gov.au/Record/1869235/Copyright.
[36] S. Södergren, A. Hagfeldt, J. Olsson and S. Lindquist, "Theoretical models for the action spectrum and the current–voltage characteristics of microporous semiconductor films in photoelectrochemical cells", *J. Phys. Chem.* **98** (1994) 5552–5556; doi:10.1021/j100072a023.
[37] V. Thomée, *Galerkin finite element methods for parabolic problems*, Volume 25 of *Springer Ser. Comput. Math.* (Springer, Berlin–Heidelberg, 2006); doi:10.1007/3-540-33122-0.
[38] Z. Tomovski and T. Sandev, "Exact solutions for fractional diffusion equations in a bounded domain with different boundary conditions", *Nonlinear Dynam.* **71** (2013) 671–683; doi:10.1007/s11071-012-0710-x.
[39] Q. Yuan and H. Chen, "An expanded mixed finite element simulation for two-sided time-dependent fractional diffusion problem", *Adv. Differential Equations* **2018** (2018) Article ID 34; doi:10.1186/s13662-018-1483-4.
[40] S. B. Yuste and L. Acedo, "An explicit finite difference method and a new von-Neumann-type stability analysis for fractional diffusion equations", *SIAM J. Numer. Anal.* **42** (2005) 1862–1874; doi:10.1137/030602666.
[41] W. K. Zahra and S. M. Elkholy, "The use of cubic splines in the numerical solution of fractional differential equations", *Int. J. Math. Math. Sci.* **2012** (2012) 638026; doi:10.1155/2012/638026.